Carbon dioxide (CO$_2$) concentrations and emission in the newly constructed Belo Monte hydropower complex in the Xingu River, Amazonia

Kleiton R. Araújo[1*], Henrique O. Sawakuchi[2-3], Dailson J. Bertassoli Jr.[4], André O. Sawakuchi[1,4], Karina D. da Silva[1,5], Thiago V. Bernardi[1,5], Nicholas D. Ward[6-7], Tatiana S. Pereira[1,5].

[1]Programa de Pós Graduação em Biodiversidade e Conservação, Universidade Federal do Pará, Altamira, 68372 – 040, Brazil,

[2]Centro de Energia Nuclear na Agricultura, Universidade de São Paulo, Piracicaba, Brazil,

[3]Department of Ecology and Environmental Science, Umeå University, Umeå, SE-901 87, Sweden,

[4]Departamento de Geologia Sedimentar e Ambiental, Instituto de Geociências, Universidade de São Paulo, São Paulo, Brazil,

[5]Faculdade de Ciências Biológicas, Universidade Federal do Pará, Altamira, 68372 – 040, Brazil,

[6]Marine Sciences Laboratory, Pacific Northwest National Laboratory, Sequim, Washington, 98382, USA,

[7]School of Oceanography, University of Washington, Seattle, Washington, 98195-5351, USA.

Correspondence to: Kleiton R. Araújo (kleitonrabelo@rocketmail.com)

Keywords: run-of-the-river reservoir; greenhouse gas emission; tropical river damming.

Abstract

The Belo Monte hydropower complex located in the Xingu River is the largest run-of-the-river (ROR) hydroelectric system in the world and has one of the highest energy production capacities among dams. Its construction received significant media attention due to its potential social and environmental impacts. It is composed of two ROR reservoirs; the Xingu Reservoir (XR) in the Xingu's main branch and the Intermediate Reservoir (IR), an artificial reservoir fed by waters diverted from the Xingu River with longer water residence time compared to XR. We aimed to evaluate spatiotemporal variations of CO_2 partial pressure (pCO_2) and CO_2 fluxes (FCO_2) during the first two years after the Xingu River impoundment under the hypothesis that each reservoir has contrasting FCO_2 and pCO_2 as vegetation clearing reduces flooded areas emissions. Time of the year had a significant influence on pCO_2 with the highest average values observed during the high water season. Spatial heterogeneity throughout the entire study area was observed for pCO_2 during both low and high water seasons. FCO_2, on the other hand only showed significant spatial heterogeneity during the high water period. FCO_2 (0.90 ± 0.47 and 1.08 ± 0.62 μmol m^2 d^{-1} for XR and IR, respectively) and pCO_2 ($1,647 \pm 698$ and $1,676 \pm 323$ μatm for XR and IR, respectively) measured during the high water season were on the same order of magnitude as previous observations in other Amazonian clearwater rivers unaffected by impoundment during the same season. In contrast, during the low water season FCO_2 (0.69 ± 0.28 and 7.32 ± 4.07 μmol m^2 d^{-1} for XR and IR, respectively) and pCO_2 (839 ± 646 and $1,797 \pm 354$ μatm for XR and IR, respectively) in IR were an order of magnitude higher than literature FCO_2 observations in clearwater rivers with naturally flowing waters. When CO_2 emissions are compared between reservoirs, IR emissions were 90% higher than values from the XR during low water season, reinforcing the clear influence of reservoir characteristics on CO_2 emissions. Based on our observations in the Belo Monte hydropower complex, CO_2 emissions from ROR reservoirs to the atmosphere are in the range of natural Amazonian rivers. However, the associated reservoir (IR) may exceed natural river emission rates due to the pre-impounding vegetation influence. Since many reservoirs are still planned to be constructed in the Amazon and throughout the world, it is critical to evaluate the implications of reservoir traits on FCO_2 over their entire life cycle in order to improve estimates of CO_2 emissions per KW for hydropower projects planned for tropical rivers.

1 Introduction

Rivers and streams are no longer considered passive pipes where terrestrial organic matter (OM) travels unchanged from land to sea (Cole et al., 2007). The OM transported by inland waters may be converted to carbon dioxide (CO_2) or methane (CH_4) and escape to the atmosphere as gaseous emissions (Battin et al., 2009; Ward et al., 2013). Inland waters cover an approximate area of 4.6 to 5 million km² or about 3% of Earth's land surface (Downing et al., 2006; Verpoorter et al. 2014). Roughly 5.1 Pg C y^{-1} of carbon is mobilized into inland waters from the terrestrial biosphere (Drake et al. 2017), of which about 2.1 Pg C y^{-1} is emitted to the atmosphere as CO_2 (Raymond et al., 2013). Despite the relatively small area covered by inland waters, their carbon emissions offset the ocean's carbon sink (1.42 ± 0.53 Pg C y^{-1}) (Landchützer et al., 2014).

Channel impoundment promotes several changes in river properties such as surface wind shear, water temperature, discharge and turbulence, and organic and inorganic sediment input (St. Louis et al., 2000). These changes alter the microbial community structure and biogeochemical processes in the water column and riverbed sediments, with consequent impacts on the dissolved carbon load, production, and eventual release to the atmosphere as CO_2 (Battin et al., 2008). The intense decomposition of OM contained in flooded soils, in addition to the consumption of allochthonous OM deposited in the reservoir may lead to an increase of the CO_2 production, and outgassing, particularly during the first years of channel impoundment (Guérin et al., 2006). Longer water residence time and reduction in water flow velocity, on the other hand, may increase light penetration depth due to the deposition of suspended sediments, possibly counterbalancing those emissions due to higher CO_2 uptake by primary producers (Duarte and Prairie, 2005). Alternatively, this condition may stimulate OM decomposition via photo-oxidation that is favored by increased light absorbance (Miller and Zepp, 1995) and microbial priming effects driven by interactions between allochthonous and autochthonous carbon sources (Ward et al., 2016).

Some of the hydropower dams' impacts may be minimized according to the dam design. Run-of-the-river (ROR) hydropower systems maintain a similar flow to a natural river (Csiki and Rhoads, 2010), which generates smaller reservoirs that operate according to seasonal variations in water levels (Egré and Milewski, 2002). The Belo Monte hydropower complex in the lower Xingu River operates as ROR and it is the largest hydropower plant in the Amazon. It ranks third in the world in terms of installed capacity (11,233 MW), but with high variation in energy production throughout the year due to the high seasonality of the water discharge of the Xingu River (EPE, 2009). Significant debate has surrounded the Belo Monte hydropower project since its initial survey in the 1980s due to the magnitude of the environmental impact and threat to local indigenous people (Fearnside, 2006). These discussions lasted at least 20 years and resulted in a series of changes and revisions to the initial project (Fearnside, 2006). Nevertheless, the Belo Monte hydropower complex had its reservoirs filled in 2015 (MME, 2011), amid strong environmental controversies (Fearnside, 2017), including uncertainties in estimates of greenhouse gas (GHG) emissions (Fearnside, 2002). As such, alterations in the natural carbon cycling in the aquatic environments under direct and indirect influence of the Belo Monte hydropower facilities may result in significant impacts on the regional carbon budget. This is a critical question to evaluate the GHG emissions related with hydroelectricity produced from impoundment of large tropical rivers.

Hundreds of new hydropower reservoirs are currently under construction or planning stages in tropical South America, Africa, and Asia (Winemiller et al., 2016), and many of them may be ROR reservoirs. However, to our knowledge, estimates of GHG emissions from ROR reservoirs only include measurements performed several decades after the construction of a small temperate reservoir in Switzerland, or obtained through modeling for tropical reservoirs in Brazil (DelSontro et al., 2010; Faria et al., 2015). Therefore, most of the GHG emissions estimates available in the literature are for storage reservoirs, but also with measurements representative of

80   several years (> 10 years) after the construction of the hydropower dams (Kemenes et al., 2011; Lima et al., 2002). Exceptions are a tropical (Abril et al., 2005) and a boreal storage reservoirs (Teodoru et al. 2011) studied since impoundment. These studies showed that CO_2 emissions were higher during the first years of impoundment. Thus, estimates of GHG emissions immediately after river impoundment are critical determining the overall carbon balance of the hydroelectricity system lifetime.

85   The Belo Monte hydropower plant has two reservoirs operating under ROR conditions. The Xingu Reservoir (XR) was formed by the impoundment of the Xingu River channel, which has waters diverted to feed the Intermediate reservoir (IR), created by the impoundment of a valley artificially connected to the left margin of the Xingu River. Although both reservoirs are considered to be ROR, they differ in water residence time and type of flooded vegetation and substrates. Flooded areas in the XR correspond mainly to seasonally flooded forest, but upland

90   forest in marginal areas was also flooded locally. Vegetation was removed from most of the flooded areas, but part of the flooded forest islands in the XR was not cleared. On the other hand, the IR flooded large swaths of upland forest and pasture areas and its water residence time is higher than in the XR.

The aim of this study is to evaluate CO_2 emissions from the Belo Monte hydropower complex during the first two years post-impoundment by assessing the spatial and temporal variability CO_2 partial pressure (pCO$_2$) and CO_2

95   fluxes (FCO$_2$) in the XR and IR. This evaluation is crucial to understand GHG emissions from reservoirs in the eastern Amazon, a tropical region poised to add 153 more hydropower facilities in the coming decades (Aneel, 2019). Considering the physiographic and hydraulic differences of the XR and IR, we hypothesize that (1) the two Belo Monte reservoirs have contrasting pCO$_2$ and FCO$_2$; and (2) the clearing of forest vegetation significantly reduces the emissions from areas flooded by the reservoirs during the first two years after channel impoundment.

100   2 Material and methods

2.1 Study area

The Xingu River is the second largest clearwater tributary of the Amazon River. It drains an area of 504,000 km^2 and flows from central Brazil (15°S) to the lower Amazon River in eastern Amazon (3°S) (Latrubesse et al., 2005; Eletrobrás, 2009a). Clearwater rivers are characterized by neutral to slightly alkaline pH, and low concentration of

105   suspended sediment, with high light penetration (Sioli, 1984). The climate of the region has high seasonality, with the rainy period usually starting in December, extending until May and rainfall peaking in March and April (Inmet, 2017). The dry season occurs from June to November, with the driest months occurring in September and October (Fig.1). The average monthly rainfall and temperature were 188 ± 145 mm and 27.5 ± 1.0 °C, respectively (10 year average from 2004 to 2014) (Inmet, 2017). In accordance with the rainfall regime, river

110   discharge is marked by strong seasonality with the low water season occurring from September to November, and the high water season from March to May. The historic average discharge of the Xingu River in the sector of the Belo Monte hydropower complex for the period from 2004 to 2014 was 1,408 ± 513 m³ s^{-1} during the low water season and 18,983 ± 9,228 m³ s^{-1} in the high water season (Fig.1) (ANA, 2017). The dominant land cover in the middle and lower Xingu watershed is tropical rainforest, although agriculture and deforested areas occur

115   mainly in the south and southwest areas of the basin and close to Altamira, the largest city near the Belo Monte hydropower complex (Eletrobrás, 2009a). The studied area ranges from the lower Iriri River, the largest tributary of the Xingu River, to downstream of the sector known as "*Volta Grande do Xingu*" (Xingu Great Bend), nearby the municipality of Vitória do Xingu(Fig. 2).

The construction of Belo Monte started in 2011, and reservoirs (Fig. 2) were flooded in 2015 (EPE, 2011). The

120   studied reservoirs have maximum depths reaching 20.5 m in the XR and 58.3 m in the IR, although both dams have similar intake depths of about 15-20 m. The Pimental dam in the Xingu River channel hosts 6 turbines and floodgates that regulate the water flow from the XR through a 28 km channel to feed the IR formed by the Belo

Monte dam. The latter contains the main power station with 18 turbines summing 11,000 MW of potential energy production, equivalent to 97% of the total installed power capacity of 11,233 MW (Eletrobrás, 2009b; EPE, 2009).

Together the reservoirs occupy an area of 516 km². The XR extends over an area of 382 km^2 (Eletrobrás, 2009a) from which 94 km^2 corresponds to land permanently or seasonally flooded, similar to the natural water level condition during the high water season (Fig.2). It is estimated that 52% of the total area flooded by the XR was not cleared of vegetation (Norte Energia, 2015). Differently, the IR occupies an area of 134 km^2 and large flooded areas of pasture and upland non-flooded forest (locally called "*terra firme* forest"). Contrary to the XR, the IR flooded area was totally vegetation cleared previously to reservoir filling (Norte Energia, 2015). Waters diverted from the XR return to the Xingu River channel after flowing around 34 km over flooded lands in the IR (Fig.2) (Eletrobrás, 2009b; EPE, 2009). The sector of the Xingu River between the outflows of the XR and IR, including part of the Xingu Great Bend, has reduced water discharge and flow controlled by operational conditions of the Belo Monte hydropower complex.

The residence times (RT) of the XR and IR were calculated based on the maximum potential discharge established for each dam (Eletrobrás, 2009a). We assumed that the sum of both discharges is the total discharge in an extreme scenario, and therefore equivalent to the fraction of the total river discharge passing through each dam. The fraction of discharge was combined with the historical average annual discharge of the Xingu River (ANA, 2017), similarly to Faria et al. (2015), using the following Eq. (1):

$$RT = \frac{V}{Q} \tag{1}$$

Where RT is the water residence time given in seconds, and later converted into days, V is the reservoir volume in m^3 and Q is the volumetric discharge in m^3/s. The XR has RT of 3.4 days while RT in the IR is 20.2 days. This difference was used to test if the RT plays a significant role in the CO_2 emissions in ROR reservoirs.

2.2 pCO$_2$ and FCO$_2$ to the atmosphere

In order to cover zones with different flooded substrates and hydrologic characteristics, the sampling sites included the original river channel within the XR, flooded lands (forest and pasture) of both reservoirs, and upstream and downstream river channel sections outside the influence of the reservoirs (Fig.2). Four classes were considered to evaluate the spatial heterogeneity of FCO_2:

(I) unaffected river channel: sites located in the channels of the Xingu and Iriri Rivers outside reservoir areas, in sectors upstream and further downstream of the reservoirs;

(II) main channel: Xingu River main branch within the reservoir area (XR);

(III) flooded areas: lands of pasture and upland forest formerly non-flooded during the high water level season and seasonally-flooded forested islands that were permanently inundated by both reservoirs;

(IV) downstream of the dams: sites immediately downstream of the dams that receive the water discharge from turbines of the XR and IR dams.

Sampling sites near the confluence of the Xingu and Iriri Rivers (sites P1 and P3, Table 1) were used as reference sites for areas without direct influence of the reservoirs. The sites further downstream of the dams (P20 and P21) were characterized to investigate the influence of the reservoirs on the downstream FCO_2 (Table 1).

During the year of 2017 (high and low water level seasons), values of pCO_2 in the water column were obtained using the headspace equilibration method according to Hesslein et al. (1991). The pCO_2 was measured following three depth classes (Table 1): (I) near bottom: 0.5-1.0 m above the river or reservoir bottom; (II) 60%: at 60% of total water depth; (III) surface: up to 0.3 m of water depth. Sites shallower than 7.5 m were sampled only at 60 % of the total depth. Polycarbonate bottles of 1 L were overflowed three times their volume with water drawn by a

submersible pump. The bottle was closed with rubber stopper adapted with tubes and luer-lock valves, allowing the simultaneous injection of 60 mL of atmospheric air and withdrawal of the same volume of water using syringes, creating the headspace. The bottles were shaken for three minutes to equilibrate the gas in the water and headspace air. Water was then re-injected simultaneously to the collection of the headspace air.

170 Atmospheric air samples were also collected using 60 ml syringes for corrections related with atmospheric CO_2. All gas samples were transferred from syringes to glass vials that were pre-capped with butyl rubber stoppers and evacuated with a vacuum pump. pCO_2 was measured using a Picarro® G2201-i cavity ring-down spectroscopy (CRDS) and concentration calculations were based on Wiesenburg and Guinasso (1979).

Diffusive CO_2 emission was measured with floating chambers during 2016 and 2017 high water seasons using an
175 infrared gas analyzer (IRGA) LI-COR® Li820 coupled to a 7.7 L opaque (covered with reflexive aluminum tape) floating chamber with 0.08 m^2 of area and 11.7 cm of height. The analyzer captures the change in CO_2 concentration inside the chamber by constant recirculation driven by a micro-pump with an air flow of 150 mL min^{-1}. For each site, three consecutive deployments were made for five minutes each from a drifting boat to avoid extra turbulence. During the 2017 low water season CO_2 mini-loggers (Bastviken et al., 2015) placed inside 6 L
180 opaque (covered with reflexive aluminum tape) floating chambers with 0.07 m^2 of area and 10.5 cm of height were used to measure FCO_2. Sensors were placed inside the two chambers and deployed simultaneously during 20-30 minutes with a logging frequency of 30 seconds. FCO_2 from water to the atmosphere were calculated according to Frankignoulle et al. (1998):

$$FCO_2 = \left(\frac{\delta pCO_2}{\delta t}\right)\left(\frac{V}{RT_K A}\right), \tag{2}$$

185 The FCO_2 in mol CO_2 m^{-2} s^{-1} is given by the changes in pCO_2 inside the chamber during the deployment time ($\delta pCO_2/\delta t$, µatm s^{-1}), taking into account the chamber volume (V, m³), the universal gas constant (R, atm m^3 mol^{-1} K^{-1}), water temperature (T, K) and the area covered by the chamber (A, m^2). Measurements were discarded when the R^2 of the linear relation between pCO_2 and time ($\delta pCO_2/\delta t$) were lower than 0.90 ($R^2 < 0.90$) or had negative FCO_2 values with surface pCO_2 higher than atmospheric pCO_2 measured on site. The gas sampling
190 survey (Fig.2 and Table 1) occurred during the high water level season in April 2016, May 2017 and during the low water level season in September 2017. Due to technical difficulties, pCO_2 data were only collected during 2017 and FCO_2 samplings of 2017 were made with different equipment.

2.3 Gas transfer velocity (k_{600})

The air-water gas transfer coefficient k (cm h^{-1}) of CO_2 was estimated based on the surface water CO_2
195 concentration inside the floating chamber by Eq. (3):

$$k = \frac{V}{A.\alpha}\ln\left(\frac{pCO_{2w}-pCO_{2i}}{pCO_{2w}-pCO_{2f}}\right)/(t_f - ti), \tag{3}$$

Where V and A are the chamber volume (cm³) and area (cm²), α is the Ostwald solubility coefficient (dimensionless), t is the time (h), and the subscripts w, i and f refers to the partial pressure in the surface water, and initial and final time inside the chamber, respectively. Ostwald solubility coefficient was calculated from K0 as
200 described by Wanninkhof (2009). Finally, k values were normalized to k_{600} following the Eq. (4) and (5) (Alin et al., 2011; Jähne et al., 1987; Wanninkhof, 1992):

$$k_{600} = k_T\left(\frac{600}{Sc_T}\right)^{-0.5}, \tag{4}$$

Where k_T is the measured k value at in situ temperature (T), Sc_T is the Schmidt number calculated from temperature and 600 is the Schmidt number for temperature of 20° C. The Schmidt number is calculated as a temperature (T) function:

$$Sc_T = 1911.1 - 118.11\,T + 3.4527\,T^2 - 0.041320\,T^3, \tag{5}$$

2.4 Physical-chemical characteristics

Depth profiles with a measurement interval of 1m were done for water temperature, pH, dissolved oxygen (DO) and conductivity using a multiparameter probe (EXO2®, YSI). During the high water in 2016 and 2017 sampling campaigns, technical challenges prevented measurement of pH, dissolved oxygen (DO), and conductivity during the 2017 low water sampling. For statistical analysis these measurements were selected following the same water depth classes applied to pCO_2 measurements (surface, 60% and near the bottom). Additionally, air temperature and wind speed were measured at the same time of chamber deployments with a handheld meteorological meter (Kestrel[®] 5500) positioned at 2 m above the water surface.

2.5. Statistical analysis

Statistical analyses were performed to check the correlation among CO_2 variables (FCO_2 and pCO_2) and water column characteristics (pH, dissolved oxygen (DO) and water temperature) and to evaluate the spatial and seasonal variation of FCO_2, pCO_2 and k_{600}. Normality and heterogeneity of variance were not achieved by Shapiro-Wilks and Bartlett tests, respectively. Thus, non-parametric and multivariate statistical tests were used. The seasonal and spatial variability of FCO_2, pCO_2, k_{600} and wind velocity were tested by PERMANOVA analysis (Anderson, 2001), a multivariate test that compares group variance (within and between) through a distance matrix using permutation to achieve p-value. The Euclidian index was used as distance method and 9999 permutations to run the analysis. The FCO_2 statistics were assessed separately by season due to the different sampling methods. The Spearman correlation test (Zar, 2010) was performed to evaluate the correlation between FCO_2 *versus* pCO_2, FCO_2 *versus* wind speed, k_{600} *versus* wind speed and pCO_2 *versus* physical-chemical variables (pH, DO and water temperature). All statistical analyses were performed in R (R Development Team Core, 2016) using the Vegan package (Oksanen et al., 2017) and Statistica (Statsoft 8.0) using 5% (0.05) as critical alpha for significance.

3 Results

3.1 Temporal and spatial variability in pCO_2 and FCO_2

Mean pCO_2 from areas upstream and downstream of the dams was 1,163 ± 660 µatm. Based on 2017 data pCO_2 values differed significantly between seasons ($F_{1:56}$= 9.77, R^2= 0.09, p= 0.0045) with higher pCO_2 in the high water season (1,391 ± 630 µatm) compared to the low water period (976 ± 633 µatm) (Fig. 3a). The type of environment also had a significant role in pCO_2 distribution throughout the area affected by the reservoirs ($F_{3:56}$= 13.36, R^2= 0.37, p= 0.0002). During the high water season the highest average pCO_2 was observed downstream of the dams. In contrast, during the low water season the highest average pCO_2 values were observed in the reservoirs over the flooded areas. Unaffected river channel categorized areas had the lowest pCO_2 in both seasons (Fig.3).

On average, across all seasons bottom water had higher pCO_2 (1,269 ± 689 µatm) compared to surface water (998 ± 613 µatm) ($F_{2:56}$= 4.06, R^2= 0.07, p= 0.0261) (Table 2). Surface pCO_2 was positively correlated with FCO_2 both during the high water (r= 0.80; p= 0.0009) and low water (r= 0.71; p= 0.012) seasons (Fig.3). Bottom water pCO_2 showed correlation with FCO_2 only during the high water season (r= 0.68; p= 0.042) while data from low

water season have non-significant correlation (r= 0.45; p= 0.16) (Table 3). Average FCO_2 for all sites sampled during 2016 and 2017 high water seasons was 1.38 ± 1.12 µmol CO_2 m^{-2} s^{-1} with similarity between years ($F_{1:28}$= 0.09, R^2= 0.01, p= 0.7790). Therefore, FCO_2 data from the high water seasons of 2016 and 2017 were treated as a single data set for the further calculations.

The highest (12.00 ± 3.21 µmol CO_2 m^{-2} s^{-1}) and lowest (-0.52 µmol CO_2 m^{-2} s^{-1}) FCO_2 values were observed during the low water season (Fig.3). Significant difference in FCO_2 was observed among environments sampled during high water season ($F_{3:28}$= 7.94, R^2= 0.43, p= 0.0089) while the low water season was not statistically different ($F_{3:17}$= 2.67, R^2= 0.14, p= 0.08) (Fig.4 and Table 3) considering whole study area. The highest ($2.89 \pm$ 1.74 µmol CO_2 m^{-2} s^{-1}) and lowest (0.84 ± 0.42 µmol CO_2 m^{-2} s^{-1}) average FCO_2, respectively, occurred in sectors downstream of the dams and in flooded areas sampled during the high water season. Negative FCO_2 were exclusively observed during the low water season in the river channel (Table 2 and Fig.4).

In addition to the spatial heterogeneity, pre-existing vegetation cover influenced pCO_2 and FCO_2 in the XR. Areas previously covered by pasture, upland forest and seasonally flooded forest had significantly different CO_2 concentrations. Sites that were 90 and 25 km downstream of the Pimental (XR) and Belo Monte (IR) dams, respectively, had lower pCO_2 and FCO_2 values compared to areas within the reservoirs.

3.2 pCO2 and FCO2 in the reservoirs

The spatial variability of pCO_2, FCO_2 and k_{600} were assessed within and between reservoirs. We evaluated the total CO_2 emissions from reservoirs by grouping flooded areas and river channel of the XR for comparison with flooded areas from the IR. FCO_2 and pCO_2 presented higher values in the XR during the high water season, while the opposite pattern occurred in the IR (Table 2).

XR and IR seasonal variation was not significant even when high water ($F_{1:25}$= 2.28, R^2= 0.03, p= 0.1536) and low water ($F_{2:30}$= 0.77, R^2= 0.03, p= 0.4684) seasons were evaluated separately (Table 3). pCO_2 also showed no significant difference between XR and IR ($F_{3:56}$= 0.34, R^2= 0.009, p= 0.8170). As observed for pCO_2, there was no effect of reservoir type on FCO_2 variability during high water conditions ($F_{1:28}$= 0.32, R^2= 0.01, p= 0.5811). In contrast, FCO_2 during low water condition differed significantly between XR and IR ($F_{1:17}$= 34.07, R^2= 0.61, p= 0.0003). The IR had the highest average FCO_2 (7.32 ± 4.06 µmol CO_2 m^{-2} s^{-1}) during the low water season while the XR presented low FCO_2 (0.69 ± 0.28 µmol CO_2 m^{-2} s^{-1}). Despite variations in FCO_2 and pCO_2, no difference on k_{600} was observed between reservoirs during the high water ($F_{1:9}$= 0.02, R^2= 0.01, p= 0.9180) or low water seasons ($F_{1:12}$= 5.46, R^2= 0.45, p= 0.0900) (Table 3).

3.3 Gas transfer velocity (k_{600})

The average k_{600} was 17.8 ± 10.2 and 34.1 ± 24.0 cm h^{-1} for high and low water seasons, respectively, without significant spatial heterogeneity across environments ($F_{3:9}$= 2.42, R^2= 0.70, p= 0.2043 and $F_{3:12}$= 0.12, R^2= 0.03, p= 0.9441, respectively). Values of k_{600} are correlated with wind speed (r= 0.73; p= 0.016) during the high water season, although this observation was not significant during the low water season (r= 0.53; p= 0.067).

Wind speeds ranged from 0.7 to 4.8 m s^{-1}, considering measurements for all sites and sampling periods. Highest average wind speed was observed on the river channel environment while downstream of the dams had the lowest (3.21 ± 0.89 and 1.66 ± 0.88 m s^{-1}, respectively) (Table 4). In contrast to k_{600}, wind speed varied significantly across environments ($F_{3:37}$= 6.13, R^2= 0.23, p= 0.0034), including variation between the XR and IR ($F_{2:37}$= 8.40, R^2= 0.21, p=0.0016).

3.4 Physical-chemical characteristics

The air temperatures at the studied sites varied between 27.5 and 33.8 °C during sampling in both seasons, with the maximum temperatures registered during the low water period. The surface water temperature ranged from

285   29.2 to 32.7 °C, with maximum temperature registered during the high water period. The lowest (6.60 ± 0.26) and highest (6.81 ± 0.21) average pH values, in waters of flooded areas and river channel (Table 4). The water column was relatively well-oxygenated in all studied environments, reaching average DO concentration up to 7.28 ± 0.73 mg L^{-1} in the unaffected river channel and lowest concentration in flooded areas (5.44 ± 2.00 mg L^{-1}) (Table 4). Water conductivity varied from 20.60 to 38.30 µS cm^{-1} in the studied environments, with the highest

290   average value (31.60 ± 8.63 µS cm^{-1}) recorded in flooded areas and lowest value (29.30 ± 4.85 µS cm^{-1}) in areas downstream of the dams (Table 4). In the study sites, pCO_2 is negatively and strongly correlated with pH and DO (Table 3). Correlation between pCO_2 and water temperature was absent while FCO_2 was positively correlated with wind speed (Table 3).

4 Discussion

295   ### 4.1 Temporal and spatial variability in pCO_2 and FCO_2
Although pCO_2 and FCO_2 are typically correlated (Rasera, et al., 2013), in this study we observed several examples where variability in gas transfer velocities drive variable fluxes even when pCO_2 was fairly constant. It has been shown that the amount of CO_2 in the water column and CO_2 emissions from Amazon rivers to the atmosphere vary significantly among seasons with higher fluxes generally observed during the high water season

300   (Alin et al., 2011; Rasera et al., 2013; Richey et al., 2002; Sawakuchi et al., 2017). We observed significant variability in pCO_2 between high and low water seasons, as well as in terms of physiographic-hydrologic environment, which influenced FCO_2 values. High pCO_2 production during the high water season can be related to increased input of terrestrial organic and inorganic carbon into the rivers by surface run-off and subsurface flow of water (Raymond and Saiers, 2010, Ward et al., 2017). Remaining vegetation and soils are the major sources

305   of OM in areas flooded by hydropower reservoirs that sustain high rates of CO_2 production during the initial years of impoundment (Guérin et al., 2008). In addition, the seasonal input of autochthonous and allochthonous organic material deposited in the reservoirs with higher water RT may result in seasonal pCO_2 and FCO_2 variability.

The oversaturation in CO_2 observed for XR and IR during high water conditions was spatially heterogeneous (Table 2). In the river channel environment of the XR pCO_2 decreased as FCO_2 increased and the contrary

310   occurred in flooded areas. This is perhaps due to the main OM source to the XR being standing vegetation associated with remnant flooded forests and pasture, which agrees with higher pCO_2 from flooded areas. Flooded vegetation is recognized to be the main source of OM in reservoirs, playing an important role in the CO_2 production and creating gradients of reservoir CO_2 emissions (Roland et al., 2010; Teodoru et al., 2011). The different characteristics including vegetation clearing, variation on hydrodynamic conditions, water depth

315   (Teodoru et al., 2011, Roland et al., 2010) and OM availability (Cardoso et al. 2013) may explain the difference in the observed FCO_2 and pCO_2 values.

About 59% of the XR area is the original channel of the Xingu River. However, the water velocity under reservoir conditions is slower than in channel sectors outside the effect of dams and regulated by spillways of the Pimental dam. FCO_2 measured upstream of the XR during the high water season in a sector where the channel is flowing

320   under natural conditions (Iriri River sites) was significantly higher than in the XR sector (Table 2). CO_2 concentrations in the water column may decrease, especially on upper water layers, in response to the increased photosynthetic uptake of CO_2 during lower rainfall periods (Amaral et al., 2018). During the low water season pCO_2 and FCO_2 decreased resulting in homogeneous FCO_2 likely due to photosynthetic activity in all environments, with exception of the IR (Table 2). In addition, CO_2 undersaturation relative to the atmosphere and

325   observed CO_2 uptake may be attributed to elevated primary productivity, which is facilitated due to the high light penetration and has been similarly observed in previous studies in Amazonian floodplain lakes and other clearwater rivers during the low water season (Amaral et al., 2018, Rasera et al 2013, Gagne-Maynard et al.,

2017). The occurrence of negative FCO_2 was observed only in the unaffected river channel at the furthest downstream site. This pattern can be related to the downstream decrease in suspended sediments due to increased sediment deposition in the reservoirs. FCO_2 in the XR and IR may also be favored by wind activity due to larger fetch for wave formation within the reservoirs. Wave action could favor degassing as well as the increase in suspended sediments that reduce light penetration and photosynthetic activity. These processes may also result in the observed decrease in pCO_2 and FCO_2 downstream of the dams. The site downstream of IR (P21) is within the river extent (< 30 km) that could still be affected by the reservoir similar to observations downstream of the Amazonian Balbina reservoir (Kemenes et al., 2016). However, the XR should only have a minor effect on the downstream site due to its longer distance from the dam outflow (90 km) and the presence of many large rapids and waterfalls in the Volta Grande region, quickly degassing the dissolved CO_2 coming from the upstream reservoir. The decrease in pCO_2 and FCO_2 persisted in areas downstream of the Belo Monte reservoirs as indicated by measurements performed in this study during the high water and low water seasons. The river reaches downstream of the Belo Monte dams have CO_2 emissions similar to observations from previous studies with emissions also decreasing downstream (Abril et al. 2005; Kemenes et al. 2011).

River reaches downstream of tropical storage reservoirs FCO_2 measured in the Sinnamary River downstream of the Petit Saut reservoir in French Guiana was 10.49 ± 3.94 µmol CO_2 m^{-2} s^{-1} (Guérin et al. 2006), which is more than three times our average downstream FCO_2 (2.89 ± 1.74 µmol CO_2 m^{-2} s^{-1}) during high water season (Table 2). Although the Petit Saut dam has a smaller reservoir its turbine intake is hypolimnetic (Abril et al., 2005), capturing CO_2-rich bottom waters that increase downstream emissions through turbine passage (Guérin et al., 2006; Kemenes et al., 2011; 2016). Alternativelly, the Belo Monte hydropower facility operates as ROR and has waters mixed without stratification and lower CO_2 oversaturation than in the Petit Saut reservoir likely due to vegetation clearing.

4.2 pCO_2 and FCO_2 on Belo Monte reservoirs

The IR presented an average FCO_2 about 90% higher than values observed in the XR during low water season. Although the XR has a larger surface area than the IR (excluding the water diversion channel), most of it corresponds to the natural river channel under a hydraulic condition similar to the high water season with less flooded areas, restricted to narrow upland margins, but including flooded large forested islands. On the other hand, the higher flooded area extension of the IR was previously covered by upland forest and pasture resulting in higher organic matter availability. CO_2 emissions from the IR during the low water season were even above the range of emissions observed in storage reservoirs in the Amazon such as the Tucuruí hydropower complex, built in 1984 on the clearwater Tocantins River (Lima et al. 2002). After more than 30 years the Tucuruí reservoir still contributes with 3.61 ± 1.62 µmol CO_2 m^{-2} s^{-1} to the atmosphere (Lima et al., 2002). In comparison to the XR ($FCO_2 = 0.69 \pm 0.28$ µmol CO_2 m^{-2} s^{-1}) the Tucuruí reservoir has higher FCO_2. However, this is three times lower than FCO_2 (7.32 ± 4.06 µmol CO_2 m^{-2} s^{-1}) measured in the IR during the low water season.

Some characteristics of the Tucuruí reservoir such as the lack of vegetation clearing prior to flooding and large reservoir area contribute to its relatively high GHG emissions (Fearnside, 2002). It must be considered that XR had partial vegetation removal in some areas, while IR had its entire landscape cleared. FCO_2 and pCO_2 measured during high water conditions in the Belo Monte reservoirs area (Table 2) were in the same order of magnitude of emissions measured in Amazon clearwater rivers unaffected by impoundment including the Tapajós River, which has hydrologic conditions similar to the Xingu River (Table 5) (Alin et al., 2011; Rasera et al., 2013; Sawakuchi et al., 2017). The vegetation clearing possibly maintained the low CO_2 emissions on both reservoirs during high water. However, the CO_2 emission from the IR is higher during low water, exceeding the fluxes of the Amazon River (Table 2) (Table 5). When analyzed separately, average FCO_2 values observed for

XR and IR overcome these natural emissions. Based on the Belo Monte case, ROR dams are a CO_2 source to the atmosphere similar to natural rivers during high water season. However, the associated reservoir may promote increased CO_2 emission during the low water season compared to natural emissions from river channels.

375   Our highest FCO_2 were observed in the IR during the low water season, which is in contrast to previous observations in other tropical and subtropical reservoirs in China and French Guiana (Abril et al. 2005; Wang et al., 2015). In the aforementioned reservoirs lower pCO_2 was observed during the low water season, which was attributed to high photosynthetic rates in the epilimnion. pCO_2 in the XR and other sites outside the reservoirs in the Xingu River also showed lower pCO_2 during the low water season, indicating that higher fluxes may have

380   been mitigated by enhanced primary productivity caused by reduced turbidity. Residence time can also play an important role on pCO_2. For example, the Three Gorges reservoir has a peak in pCO_2 and low Chlorophyll-*a* concentrations during summer and spring seasons when RT is the lowest (Li et al., 2017). In this case the reservoir type (river-type) directly influences water mixing and consequently the RT, similar to the differences observed here between the IR and XR. In low RT reservoirs, nitrogen and phosphorous may not be the limiting

385   factor to phytoplankton growth and it may be restricted by the high flow (Xu et al. 2011). The deficit in CO_2 consumption related to an underperforming phytoplankton community may point to a misbalanced sink in the reservoir carbon balance that remains poorly understood.

CO$_2$ emissions may be correlated with prior vegetation flooding with higher FCO_2 occurring in areas with the highest carbon stocks such as forests and wetlands (Teodoru et al., 2011). Although vegetation was cleared in

390   the IR before flooding, the upper soil layer may have kept a high concentration of plant-derived material fuelling emissions. This condition explains the higher average pCO_2 in IR compared to XR with the former area also having higher average FCO_2 values. The XR has substrates with relatively reduced carbon storage because almost half of the area represents the original river channel dominated by bedrock or sandy substrates and islands formed by sand and mud deposition, which would not store as much carbon (Sawakuchi et al., 2015).

395   4.3 Gas transfer velocity (k_{600})

Although no significant difference of k_{600} was observed between the reservoirs of the Belo Monte hydropower complex, the observed gas transfer velocities vary among different environment types. The XR had gas transfer velocities in the range of the Furnas reservoir in the Grande River draining the Cerrado biome (savanna), which has a k_{600} of 19.6 ± 2.5 cm h^{-1} (Paranaíba et al., 2017). This value is similar to k_{600} values obtained in this study

400   for the XR (23.0 ± 8.0 and 22.9 ± 21.4 cm h^{-1} during high and low water seasons, respectively). In contrast, the IR had a k_{600} of 7.1 ± 1.5 cm h^{-1} (high water), which resembles gas transfer velocities of the Lagoa Grande de Curuai (6.0 cm h^{-1}, following Cole and Caraco wind-based model) (Rudorff et al., 2011) in the floodplain of the Amazon River. We observed that in the XR reservoir area, FCO_2 values were higher in the main channel environment. In addition, the relatively stable water flow due to the ROR type reservoir also had a large fetch

405   area for wave formation in comparison with the sheltered flooded areas in bays and small tributaries. This is consistent with the positive correlation observed between wind speed and FCO_2 here and in other large rivers where a vast water surface interacts with wind along its fetch, promoting the formation of waves that enhances water turbulence, k_{600} and FCO_2 (Abril et al., 2005; Paranaíba et al. 2017; Rasera et al., 2013; Raymond and Cole, 2001; Vachon et al., 2013). In addition, at the low water season the elevated gas transfer coefficients

410   coupled with the short water residence time suggests that the system has a strong influence of water turbulence on k_{600}.

5 Conclusions

In this study, we observed significant variability in FCO_2 related to the type of fluvial environment and land use of areas flooded by the reservoirs of the Belo Monte hydropower complex. The observed CO_2 emissions were 90% higher for the IR compared to XR during low water season indicating that flooded land and higher residence time may play an important role on CO_2 emissions to the atmosphere even in ROR reservoirs. Our measurements comprise the first two years after reservoir filling, which is a critical period to assess GHG emissions from reservoirs. During the high water season, the XR had average CO_2 emissions similar to Amazonian clearwater rivers without impounding and considerably lower emissions than several other tropical reservoirs that have been studied. However, CO_2 emissions during the low water season were higher than natural emissions and the IR FCO_2 exceeded emissions measured in storage reservoirs of other tropical rivers. ROR reservoirs alter CO_2 emissions compared to naturally flowing Amazonian clearwater rivers, except when installed on the main river channel. On upland forested areas ROR reservoirs can experience significantly increased CO_2 production rates due to pre-impoundment vegetation and soil organic matter. Despite vegetation removal the IR had the highest FCO_2 observed in this study. Although vegetation removal is considered an effective approach for reducing GHG emissions from hydropower reservoirs we show that tropical reservoirs can still have significant emissions even after vegetation suppression. A long-term monitoring of GHG emissions of Belo Monte working at full capacity and including a more detailed assessment of the downstream sections of the reservoirs is needed to obtain a robust estimate of carbon emissions related to the energy produced by the Belo Monte hydropower complex over its entire lifecycle.

Author contribution

Kleiton R. Araújo collected and analyzed the data and prepared the manuscript with the contribution of all co-authors. Henrique O. Sawakuchi designed the study, cooperated in the field sampling and supported with guidance on data analysis. Dailson J. Bertassoli Jr. also collected the data and conducted the laboratory analysis. André O. Sawakuchi attained the grant award, contributed to setting up the field equipment, measuring infrastructure and designed the field sampling. Kleiton R. Araújo, Karina D. Silva and Thiago V. Bernardi conducted the statistical analysis. Nicholas D. Ward and Tatiana S. Pereira contributed with technical advice and guidance throughout the project implementation and paper writing stages.

Competing interests

We declare that we have no conflict of interests.

Acknowledgements

This study has funding by Fundação de Amparo à Pesquisa do Estado de São Paulo (FAPESP, grant 16/02656-9) and from Coordenação de Aperfeiçoamento de Pessoal de Nível Superior (CAPES) as master scholarship for Kleiton R. Araújo. We are grateful to Marcelo G. P. de Camargo, Hildegard de H. Silva, Victor A. T. Alem, Agna L. B. Figueiredo, and Thomas K. Akabame for the field sampling and laboratorial support. We are thankful to Oliver Lucanus for final text contributions. André O. Sawakuchi is supported by Conselho Nacional de Desenvolvimento Científico e Tecnológico (CNPq, grant 304727/2017-2). This publication was supported by Pró-Reitoria de Pesquisa e Pós-Graduação/ UFPA (PROPESP/ UFPA).

References

455   Abril, G., Guérin, F., Richard, S., Delmas, R., Galy-Lacaux, C., Gosse, P., Tremblay, A., Varfalvy, L., Dos Santos, M. A. and Matvienko, B.: Carbon dioxide and methane emissions and the carbon budget of a 10-year old tropical reservoir (Petit Saut, French Guiana), Global Biogeochem. Cycles, 19, 1–16, doi:10.1029/2005GB002457, 2005.

Alin, S. R., Rasera, M. D. F. F. L., Salimon, C. I., Richey, J. E., Holtgrieve, G. W., Krusche, A. V. and Snidvongs, A.: Physical controls on carbon dioxide transfer velocity and flux in low-gradient river systems and implications for regional carbon budgets, J. Geophys. Res.

460   Biogeosciences, 116, doi:10.1029/2010JG001398, 2011.

Almeida, C. A., Coutinho, A. C., Esquerdo, J. C. D. M., Adami, M., Venturieri, A., Diniz, C. G., Dessay, N., Durieux, L., Gomes, A. R.: High spatial resolution land use and land cover mapping of the Brazilian Legal Amazon in 2008 using Landsat-5/TM and MODIS data. Acta Amaz. 46, 291–302. doi: 10.1590/1809-43922015 05504, 2016.

Amaral, J. H. F., Borges, A. V., Melack, J. M., Sarmento, H., Barbosa, P. M., Kasper, D., de Melo, M. L., De Fex-Wolf, D., da Silva, J. S. and

465   Forsberg, B. R.: Influence of plankton metabolism and mixing depth on CO_2 dynamics in an Amazon floodplain lake, Sci. Total Environ., 630, 1381–1393, doi:10.1016/j.scitotenv.2018.02.331, 2018.

ANA: Agência Nacional Das Águas. https:// http://www.snirh.gov.br/hidroweb/publico/medicoes_historicas_abas.jsf (last acess: 27 August 2017), 2017.

Aneel: Agência Nacional de Energia Elétrica. http://www.aneel.gov.br/ (last acess: 30 May 2019), 2019.

470   Anderson, M.J.: A new method for non-parametric multivariate analysis of variance. Austral Ecology, 26, 32-46, 2001.

Bastviken, D., Sundgren, I., Natchimuthu, S., Reyier, H. and Gålfalk, M.: Technical Note: Cost-efficient approaches to measure carbon dioxide (CO_2) fluxes and concentrations in terrestrial and aquatic environments using mini loggers, Biogeosciences, 12, 3849–3859, doi:10.5194/bg-12-3849-2015, 2015.

Battin, T. J., Kaplan, L. A., Findlay, S., Hopkinson, C. S., Marti, E., Packman, A. I., Newbold, J. D. and Sabater, F.: Biophysical controls on

475   organic carbon fluxes in fluvial networks, Nat. Geosci., 2, 595–595, doi:10.1038/ngeo602, 2008.

Battin, T. J., Luyssaert, S., Kaplan, L. A., Aufdenkampe, A. K., Richter, A. and Tranvik, L. J.: The boundless carbon cycle, Nat. Geosci., 2, 598–600, doi:10.1038/ngeo618, 2009.

Cardoso, S. J., Vidal, L. O., Mendonça, R. F., Tranvik, L. J., Sobek, S. and Roland F.: Spatial variation of sediment mineralization supports differential CO_2 emissions from a tropical hydroelectric reservoir, Front. Microbiol., 4, doi: 10.3389/fmicb.2013.00101, 2013.

480   Cole, J. J., Prairie, Y. T., Caraco, N. F., McDowell, W. H., Tranvik, L. J., Striegl, R. G., Duarte, C. M., Kortelainen, P.,

Csiki, S. and Rhoads, B. L.: Hydraulic and geomorphological effects of run-of-river dams, Prog. Phys. Geogr., 34, 755–780, doi:10.1177/0309133310369435, 2010.

DelSontro, T., McGinnis, D. F., Sobek, S., Ostrovsky, I. and Wehrli, B.: Extreme methane emissions from a Swiss hydropower reservoir: contribution from bubbling sediments. Environmental science & technology, 44, 2419-2425, doi: 10.1021/es9031369, 2010.

485   Drake, T. W., Raymond, P. A. and Spencer, R. G. M.: Terrestrial carbon inputs to inland waters: A current synthesis of estimates and uncertainty, Limnol. Oceanogr. Lett., 3, doi:10.1002/lol2.10055, 2017.

Downing, J. A., Middelburg, J. J. and Melack, J.: Plumbing the global carbon cycle: Integrating inland waters into the terrestrial carbon budget, Ecosystems, 10, 171–184, doi:10.1007/s10021-006-9013-8, 2007.

Duarte, C. M. and Prairie, Y. T.: Prevalence of heterotrophy and atmospheric CO_2 emissions from aquatic ecosystems, Ecosystems, 8, 862–

490   870, doi:10.1007/s10021-005-0177-4, 2005.

Egré, D. and Milewski, J. C.: The diversity of hydropower projects. Energy Policy, 30, 1225-1230, doi: 10.1016/S0301-4215(02)00083-6, 2002.

Eletrobrás: Hydroelectric utilization of the Xingu river basin, AAI - Integrated Environmental Assessment of the Xingu River Basin, Report in portuguese, São Paulo, 204pp, 2009a.

495   Eletrobrás: Belo Monte hydroelectric power, Environmental Impact Study, Report in portuguese, Rio de Janeiro, 426pp, 2009b.

EPE: Energy Research Company - Generation epanxion bidding studies AHE Belo Monte, Technical Evaluation, Report in portuguese, Mines and Energy Ministry, Rio de janeiro, 87pp, 2009.

EPE: Energy Research Company - Ten Year Expansion Plan 2020, Final Report, Mines and Energy Ministry, Report in portuguese, Brasília, 319pp. 2011.

500   Faria, F. A. M., Jaramillo, P., Sawakuchi, H. O., Richey, J. E. and Barros, N.: Estimating greenhouse gas emissions from future Amazonian hydroelectric reservoirs, Environ. Res. Lett., 10, 124019, doi:10.1088/1748-9326/10/12/124019, 2015.

Fearnside, P. M.: Greenhouse Gas Emissions from a Hydroelectric Reservoir (Brazil's Tucuruí Dam) and the Energy Policy Impactions, 133, 69-96, doi: 10.1023/A:1012971715668, 2002.

Fearnside, P. M.: Dams in the Amazon: Belo Monte and Brazil's hydroelectric development of the Xingu River Basin, Environmental

505   management, 38, 16-27, doi: 10.1007/s00267-005-0113-6, 2006.

Fearnside, P. M.: Brazil's Belo Monte Dam: lessons of an Amazonian resource struggle. DIE ERDE–Journal of the Geographical Society of Berlin, 148, 167-184, doi: 10.12854/erde-148-46, 2017

Frankignoulle, M., Abril, G., Borges, A., Bourge, I., Canon, C., Delille, B., E., L. and Théare, J.: Carbon Dioxide Emission from European

Estuaries, Science, 282, 434–436, doi:10.1126/science.282.5388.434, 1998.

510 Gagne-Maynard, W. C., Ward, N. D., Keil, R. G., Sawakuchi, H. O., Da Cunha, A. C., Neu, V., Brito, D. C., Less, D. F. S., Diniz, J. E. M., Valerio., A. M., Kampel, M., Krusche, A., V. and Richey, J. E.: Evaluation of primary production in the lower Amazon River based on a dissolved oxygen stable isotopic mass balance. Frontiers in Marine Science, 4, doi: 10.3389/fmars.2017.00026, 2017.

Guérin, F., Abril, G., Richard, S., Burban, B., Reynouard, C., Seyler, P. and Delmas, R.: Methane and carbon dioxide emissions from tropical reservoirs: Significance of downstream rivers, Geophys. Res. Lett., 33, 1–6, doi:10.1029/2006GL027929, 2006.

515 Guérin, F., Abril, G., de Junet, A. and Bonnet, M. P.: Anaerobic decomposition of tropical soils and plant material: Implication for the CO_2 and CH_4 budget of the Petit Saut Reservoir, Appl. Geochemistry, 23, 2272–2283, doi:10.1016/j.apgeochem.2008.04.001, 2008.

Hesslein, R. H., Rudd, J. W. M., Kelly, C., Ramlal, P. and Hallard, K.: Carbon dioxide partial pressure in the surface waters of lakes in Northwestern, Ontario and the MacKenzie Delta region, Canada. in: Second International Symposium on Gas Transfer at Water Surfaces, Vicksburg, United States, August 1990, 413-431, 1991.

520 Inmet: Instituto Nacional De Meteorologia: https:// http://www.inmet.gov.br/projetos/rede/pesquisa/ (last acess in: 12 July 2017), 2017.

Jähne, B. J., Münnich, K. O. M., Bösinger, R., Dutzi, A., Huber, W. and Libner, P.: On the Parameters Influencing Air-Water Gas Exchange, J. Geophys. Res., 92, 1937–1949, doi:10.1029/JC092iC02p01937, 1987.

Kemenes, A., Forsberg, B. R. and Melack, J. M.: CO_2 emissions from a tropical hydroelectric reservoir (Balbina, Brazil), J. Geophys. Res. Biogeosciences, 116, 1–11, doi:10.1029/2010JG001465, 2011.

525 Kemenes, A., Forsberg, B. R. and Melack, J. M.: Downstream emissions of CH_4 and CO_2 from hydroelectric reservoirs (Tucurui, Samuel, and Curua-Una) in the Amazon basin, Inl. Waters, 6, 295–302, doi:10.5268/IW-6.3.980, 2016.

Landchützer, P., Gruber, N., Bakker, D. C. E. and Schuster U.: Recent variability of glolbal ocean carbon sink, Global Biogeo. Cycles, 28, 927-949, doi: 10.1002/2014GB004853, 2014.

Latrubesse, E. M., Stevaux, J. C. and Sinha, R.: Tropical rivers, Geomorphology, 70, 187-206, doi: 10.1016/j.geomorph.2005.02.005, 2005.

530 Li, S., Wang, F., Luo W., Wang, Y. and Deng, B.: Carbon dioxide emissions from the Three Gorges Reservoir, China, Acta Geochim, 36, 4, 645-657, doi: 10.1007/s11631-017-0154-6, 2017.

Lima, I. B. T., Victoria, R. L., Novo, E. M. L. M., Feigl, B. J., Ballester, B. J and Ometto, J. P.: Methane, carbon dioxide and nitrous oxide emissions from two Amazonian Reservoirs during high water table, Verhandlungen, 28, 438-442, doi: 10.1080/03680770.2001.11902620, 2002.

535 Miller, W. L. and Zepp, R. G.: Photochemical production of dissolved inorganic carbon from terrestrial organic matter: Significance to the oceanic organic carbon cycle, Geophys. Res. Lett., 22, 417-420, doi: 10.1029/94GL03344, 1995.

MME: Ministério de Minas e Energia. http://www.mme.gov.br/web/guest/destaques-do-setor-de-energia/belo-monte, (Last acess: 16 June 2019), 2019.

Norte Energia, Supressão vegetal – situação de execução, Technical Note, Superintendência dos Meios Físico e Biótico, Diretoria
540 Socioambiental, Brasília – DF, 24pp, 2015.

Oksanen, J., Blanchet, F. G., Friendly, M., Kindt, R., Legendre, P., McGlinn, D., Michin, P. R.,O'Hara, R. B., Simpson, G. L., Solymos, P., Stevens, M. H. H., Szoecs, E. and Wagner, H.: vegan: Community Ecology Package. R package version 2. 4-3. 2017.

Paranaíba, J. R., Barros, N., Mendonça, R., Linkhorst, A., Isidorova, A., Roland, F., Almeida, R. M. and Sobek, S.: Spatially resolved measurements of CO2 and CH4 concentration and gas-exchange velocity highly influence carbon-emission estimates of reservoirs, Environ.
545 Sci. Technol., 52, 607–615, doi:10.1021/acs.est.7b05138, 2018.

R Core Team. R: A Language and Environment for Statistical Computing. R Foundation for Statistical Computing, Vienna, Austria. 2016.

Rasera, M. de F. F. L., Krusche, A. V., Richey, J. E., Ballester, M. V. R. and Victória, R. L.: Spatial and temporal variability of pCO2 and CO2 efflux in seven Amazonian Rivers, Biogeochemistry, 116, 241–259, doi:10.1007/s10533-013-9854-0, 2013.

Raymond, P. A. and Cole, J. J.: Gas Exchange in Rivers and Estuaries: Choosing a Gas Transfer Velocity, Estuaries, 24, 312,
550 doi:10.2307/1352954, 2001.

Raymond, P. A. and Saiers, J. E.: Event controlled DOC export from forested watersheds, Biogeochemistry, 100, 197–209, doi:10.1007/s10533-010-9416-7, 2010.

Raymond, P. A., Hartmann, J., Lauerwald, R., Sobek, S., McDonald, C., Hoover, M., Butman, D., Striegl, R., Mayorga, E., Humborg, C., Kortelainen, P., Dürr, H., Meybeck, M., Ciais, P. and Guth, P.: Global carbon dioxide emissions from inland waters, Nature, 503, 355–359,
555 doi:10.1038/nature12760, 2013.

Richey, J. E., Melack, J. M., Aufdenkampe, A. K., Ballester, V. M. and Hess, L. L.: Outgassing from Amazonian rivers and wetlands as a large tropical source of atmospheric CO_2. Nature, 416, doi: 10.1038/416617a, 2002.

Roland, F., Vidal, L. O., Pacheco, F. S., Barros, N. O., Assireu, A., Ometto, J. P. H. B., Cimbleris, A. C. P. and Cole, J. J.: Variability of carbon dioxide flux from tropical (Cerrado) hydroelectric reservoirs, Aquat. Sci., 72, 283–293, doi:10.1007/s00027-010-0140-0, 2010.

560 Rudorff, C. M., Melack, J. M., MacIntyre, S., Barbosa, C. C. and Novo, E. M.: Seasonal and spatial variability of CO2 emission from a large floodplain lake in the lower Amazon, Journal of Geophysical Research, 116, G04007, doi:10.1029/2011JG001699, 2011.

Sawakuchi, A. O., Hartmann, G. A., Sawakuchi, H. O., Pupim, F. D. N., Bertassoli, D. J., Parra, M., J. L. Antinao, L. M. Sousa, M. H. Sabaj Pérez, P. E. Oliveira, R. A Santos, J. F. Savian, C. H. Grohmann, V. B. Medeiros, M. M. McGlue, D. C. Bicudo, and S. B. Faustino.: The Volta

Grande do Xingu: reconstruction of past environments and forecasting of future scenarios of a unique Amazonian fluvial landscape, Scientific Drilling, 20, doi: 10.5194/sd-20-21-2015, 2015.

Sawakuchi, H. O., Neu, V., Ward, N. D., Barros, M. de L. C., Valerio, A. M., Gagne-Maynard, W., Cunha, A. C., Less, D. F. S., Diniz, J. E. M., Brito, D. C., Krusche, A. V. and Richey, J. E.: Carbon Dioxide Emissions along the Lower Amazon River, Front. Mar. Sci., 4, 1–12, doi:10.3389/fmars.2017.00076, 2017.

Sioli, H.,: The Amazon and its main affluents: Hidrology, morpholy of the river courses and river types, in: The Amazon : limnology and landscape ecology of a mighty tropical river and its basin, Dr W. Junk Publishers, Netherlands, edited by: Sioli, H. and Dumont, H. J., 127 – 165, doi: 10.1007/978-94-009-6542-3, 1984.

St. Louis, V. L., Kelly, C. A., Duchemin, E., Rudd, J. W. M. and Rosenberg D. M.: Reservoir surfaces as sources of greenhouse gases to the atmosphere: a global estimate, BioScience, 5, 766-775, doi: 10.1641/0006-3568(2000)050[0766:RSASOG]2.0.CO;2, 2000.

Teodoru, C. R., Prairie, Y. T. and Del Giorgio, P. A.: Spatial Heterogeneity of Surface CO_2 Fluxes in a Newly Created Eastmain-1 Reservoir in Northern Quebec, Canada, Ecosystems, 14, 28–46, doi:10.1007/s10021-010-9393-7, 2011.

Vachon, D., Prairie, Y. T. and Smith, R.: The ecosystem size and shape dependence of gas transfer velocity versus wind speed relationships in lakes, Can. J. Fish. Aquat. Sci., 70, 1757–1764, doi:10.1139/cjfas-2013-0241, 2013.

Verpoorter, C., Kutser, T., Seekell, D. A. and Tranvik, L. J.: A global inventory of lakes based on high-resolution satellite imagery, Geophys. Res. Lett., 41, 6396–6402, doi:10.1002/2014GL060641., 2014.

Wang, F., Cao, M., Wang, B., Fu, J., Luo, W. and Ma, J. Seasonal variation of CO_2 diffusion flux from a large subtropical reservoir in East China. Atmospheric environment, 103, 129-137, doi: 10.1016/j.atmosenv.2014.12.042, 2015.

Wanninkhof, R. H.: Relationship between wind speed and gas exchange, J. Geophys. Res., 97, 7373–7382, doi:10.1029/92JC00188, 1992.

Wanninkhof, R., Asher, W. E., Ho, D. T., Sweeney, C. and McGillis, W. R.: Advances in Quantifying Air-Sea Gas Exchange and Environmental Forcing, Ann. Rev. Mar. Sci., 1, 213–244, doi:10.1146/annurev.marine.010908.163742, 2009.

Ward, N. D., Keil, R. G., Medeiros, P. M., Brito, D. C., Cunha, A. C., Dittmar, T., Yager, P. L., Krusche, A. V. and Richey, J. E.: Degradation of terrestrially derived macromolecules in the Amazon River, Nat. Geosci., 6, 530–533, doi:10.1038/ngeo1817, 2013.

Ward, N. D., Bianchi, T.S., Sawakuchi, H.O., Gagne-Maynard, W., Cunha, A.C., Brito, D.C., Neu, V., Matos Valerio, A., Silva, R., Krusche, A.V. and Richey, J. E.: The reactivity of plant-derived organic matter and the potential importance of priming effects along the lower Amazon River. Journal of Geophysical Research: Biogeosciences, 121, 1522-1539, doi: 10.1002/2016JG003342, 2016.

Ward, N. D., Bianchi, T.S., Medeiros, P. M., Seidel, M., Richey, J. E., Keil, R. G. and Sawakuchi, H. O.: Where carbon goes when water flows: carbon cycling across the aquatic continuum. Frontiers in Marine Science, 4, doi: 10.3389/fmars.2017.00007, 2017.

Wiesenburg, D. A. and Guinasso Jr, N. L.: Equilibrium solubilities of methane, carbon monoxide, and hydrogen in water and sea water. Journal of chemical and engineering data, 24, 356-360, doi:10.1021/je60083a006, 1979.

Winemiller, K. O., McIntyre, P. B., Castello, L., Fluet-Chouinard, E., Giarrizzo, T., Nam, S., Baird, I. G., Darwall, W., Lujan, N. K., Harrison, I., Stiassny, M. L. J., Silvano, R. A. M., Fitzgerald, D. B., Pelicice, F. M., Agostinho, A. A., Gomes, L. C., Albert, J. S., Baran, E., Petrere, M., Zarfl, C., Mulligan, M., Sullivan, J. P., Arantes, C. C., Sousa, L. M., Koning, A. A., Hoeinghaus, D. J., Sabaj, M., Lundberg, J. G., Armbruster, J., Thieme, M. L., Petry, P., Zuanon, J., Vilara, G. T., Snoeks, J., Ou, C., Rainboth, W., Pavanelli, C. S., Akama, A., van Soesbergen, A. and Saenz, L.: Balancing hydropower and biodiversity in the Amazon, Congo, and Mekong, Science, 351, 128–129, doi:10.1126/science.aac7082, 2016.

Xu, Y., Zhang, M., Wang, L., Kong, L., and Cai, Q. Changes in water types under the regulated mode of water level in Three Gorges Reservoir, China. Quaternary international, 244(2), 272-279, doi: 10.1016/j.quaint.2011.01.019, 2011.

Zar, J. H.: Biostatistical Analysis, 5° Ed., Pearson, New Jersey, 931 pp., 2010.

Zheng, T. G., Mao, J. Q., Dai, H. C. and Liu, D. F.: Impacts of water release operations on algal blooms in a tributary bay of Three Gorges Reservoir, Sci. China Technol. Sci., 54, 1588–1598, doi:10.1007/s11431-011-4371-7, 2011.

Figure captions

Fig.1: Average river discharge (in $m^3 s^{-1}$) of the Xingu River (left Y axis) and precipitation (in mm month^{-1}) (right Y axis) at Altamira from 2004 to 2014. Bars indicate monthly standard deviation. Data is from ANA (2017) and Inmet (2017).

Fig.2: Sampling sites upstream (Iriri river), within and downstream of the reservoirs and the location of the two dams (white bars) in the Xingu river. Black arrows indicate flow direction. Land cover data is based on the vegetation characterization from Almeida et al. (2016), where non-forested area groups pasture, deforested, secondary vegetation, and urban areas.

Fig.3: Boxplots showing the spatial and temporal variability of pCO_2 and FCO_2. Whiskers indicate standard deviation, boxes are maximum and minimum values and the middle points are mean values. High water FCO_2 (2016 and 2017 campaigns) and pCO_2 from all depths values were averaged to characterize the environmental category. Sampling sites were categorized according to river flow in un-impounded upstream (UU) to sites located upstream reservoirs, Xingu (XR) and Intermediate reservoirs (IR) that grouped sites within reservoirs area, downstream the dams (DD) that corresponded to sites directly receiving turbine outflow and un-impounded downstream (UD) related to sites further downstream with no or low reservoir influence. Temporal variation may be observed by the overall seasonal variation to pCO_2 and FCO_2 during high (A) and low water (B), likewise the spatial distribution to pCO_2 on high (C) and low water (D). Also to FCO_2 (E, F) and k_{600} (G, H) by season are disposed on high and low water, respectively.

Fig.4: Spatial and temporal variation of the FCO_2 values ($\mu mol\ CO_2\ m^{-2}\ d^{-1}$) in the reservoirs (XR and IR) of the Belo Monte hydropower complex during high water includes 2 years of data (2016 and 2017) while (A) low water only has one year (2017) (B). Black arrows indicate flow direction; colors and circle sizes indicate the type and intensity of CO_2 fluxes.

Figures

Fig.1
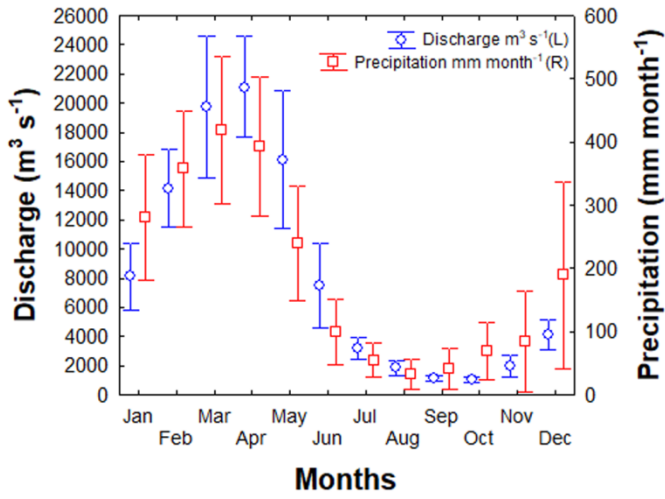
660   Fig.2

665

670

Fig.3

Fig.4

(a)

(b)

675
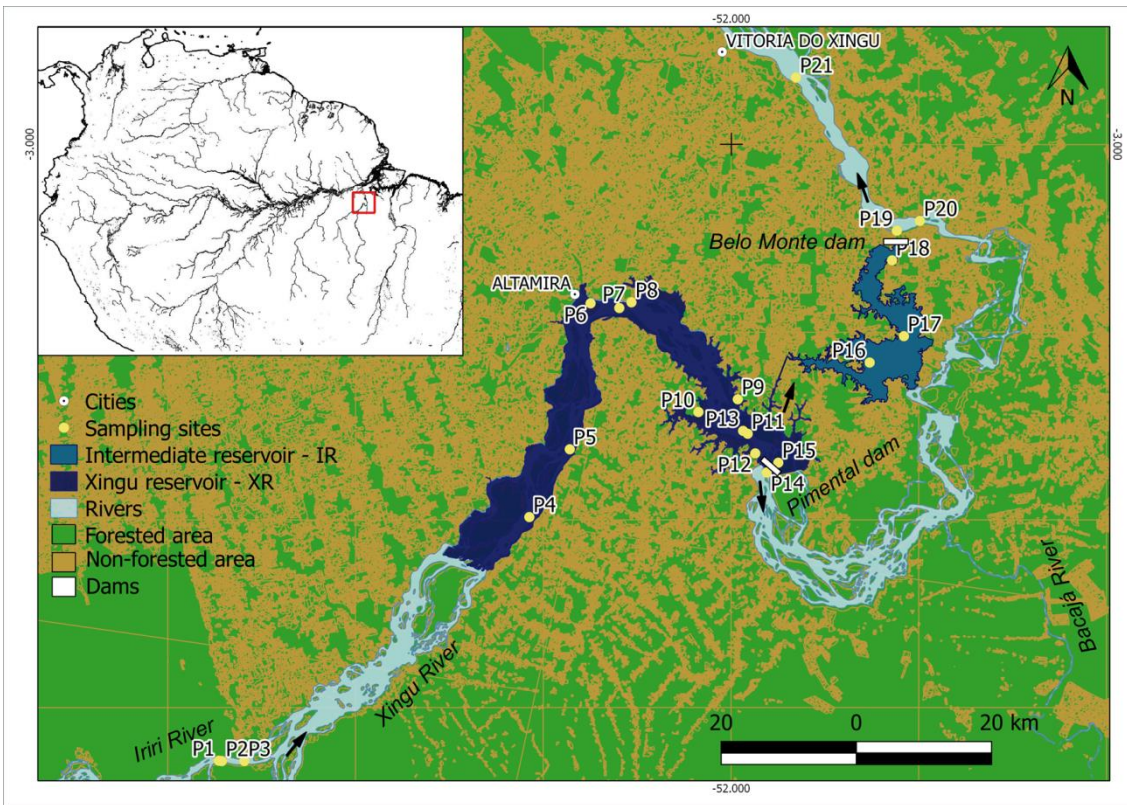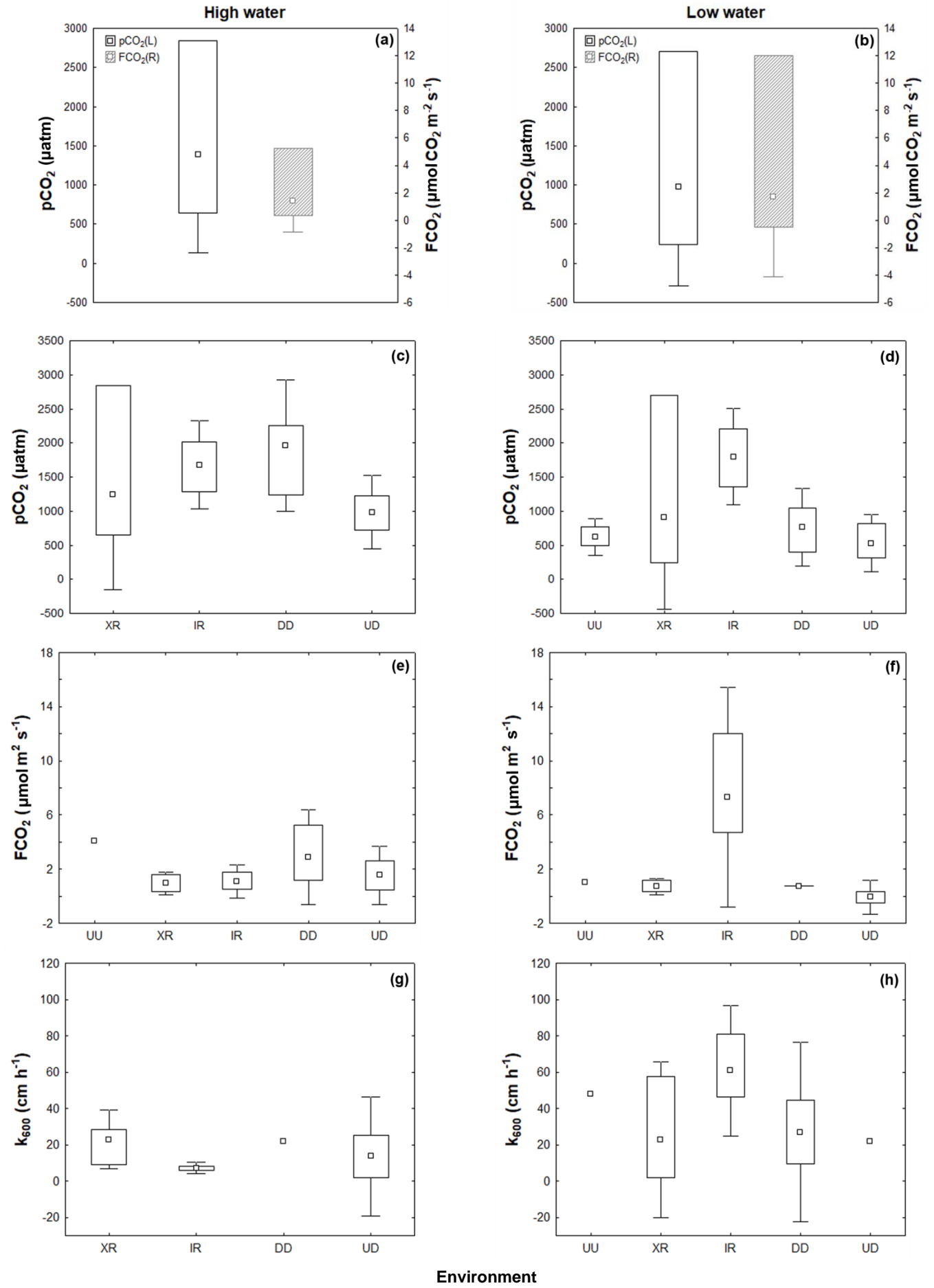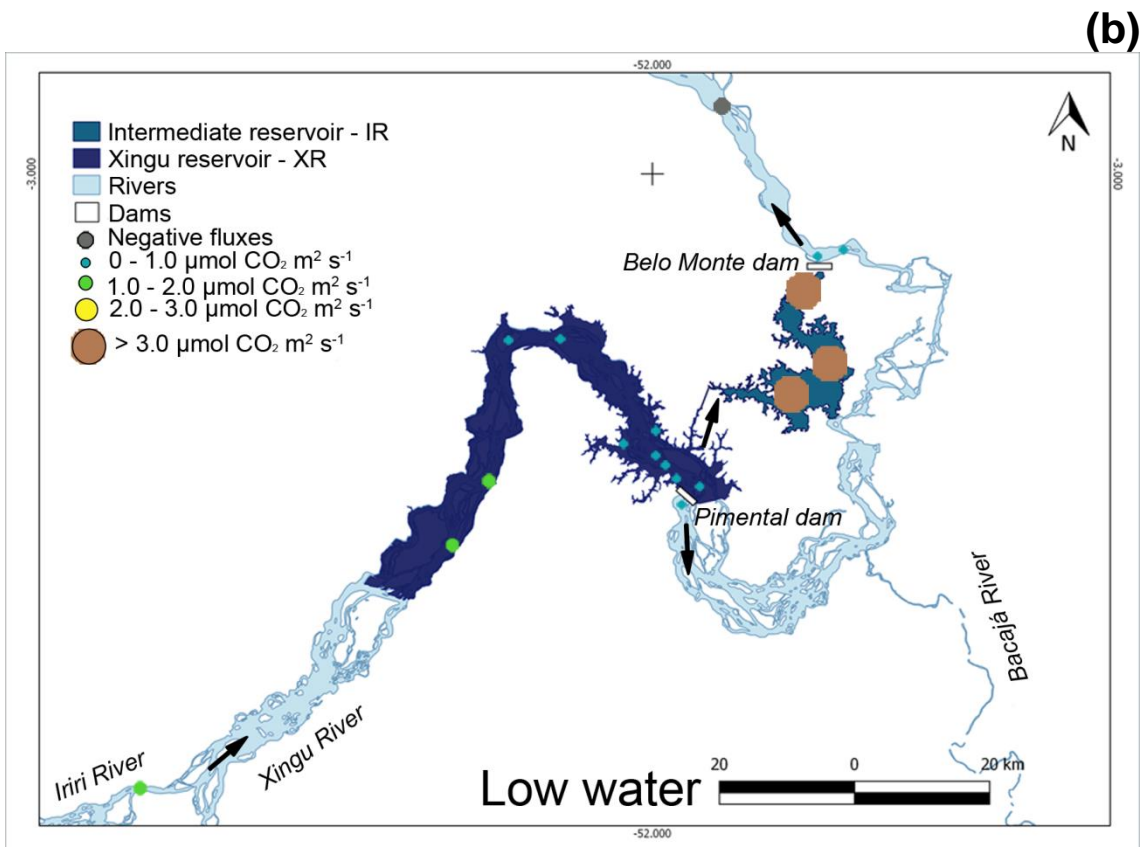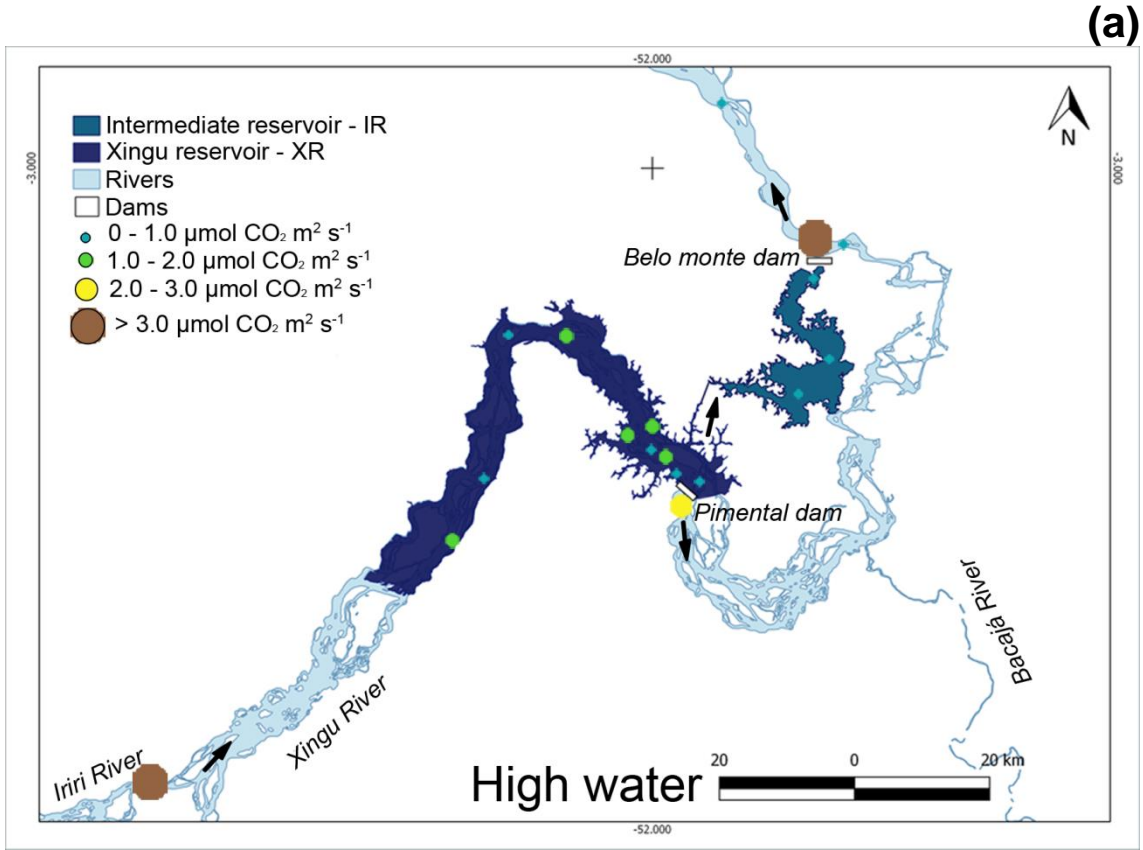
Table captions

Table 1: Locations of sampling sites in the Xingu and Iriri Rivers and reservoirs (XR and IR) of the Belo Monte hydropower complex. Sites were classified according to pre and post-flooded vegetation types, water depth and sampling season (H1: high water of 2016, H2: high water of 2017 and L: low water of 2017).

Table 2: Summary of FCO_2 in µmol CO_2 m^2 s^{-1}, pCO_2 in µatm, gas transfer velocities (k_{600}) in cm h^{-1} averages and literature values. High water season averages to FCO_2 comprehends 2016 and 2017 high water seasons since no significant variation was detected. Env = environment, Res = reservoirs, Camp = sampling campaign, Season = sampling season, and n = number of sites averaged to each variable.

Table 3: Statistical analysis results grouped by variable. The pseudo-F (F) and R² on analysis column are related to PERMANOVA test and R (Rhô) values are related to Spearman Correlation. Prefix Sur and Bot represents surface and near bottom depths, DO the dissolved oxygen and Temp the water temperature. Temporal, spatial and correlation implications of statistics are described as Effects.

Table 4: Overall physical-chemical characterization comprising the three depth classes (surface, 60% and near the bottom) sampled during the high water seasons of 2016 and 2017, with exception to Temp (water temperature) and WS (wind speed), which corresponds to both high and low water. The variables pH, DO (dissolved oxygen), Cond (conductivity), Temp, and WS (wind speed) are presented according to the environment.

Table 5: Average literature values and standard deviation of FCO_2, pCO_2, and k_{600} to Amazonian clearwater rivers according to the season. Referential values were averaged from the Amazonian clear water rivers Tapajós (Alin et al. 2011 and Sawakuchi et al. 2017), Araguaia, Javaés and Teles Pires (Rasera et al. 2013) in the correspondent season when available.

Tables

Table 1

Site	Longitude	Latitude	Pre-flooding environment	Season	Depth (m)
P1	-3.82115	-52.682559	River channel	H1	ND
P2	-3.82168	-52.678553	River channel	L	13.0
P3	-3.82153	-52.678599	River channel	L	8.0
P4	-3.49656	-52.268961	River channel	H2, L	8.1
P5	-3.40623	-52.215154	River channel	H2, L	7.5
P6	-3.21182	-52.187488	Seasonally flooded forested island	H1, H2, L	3.0
P7	-3.21801	-52.149169	River channel	H1, H2, L	20.5
P8	-3.21045	-52.133034	Pasture*	H1, H2, L	0.35
P9	-3.33965	-51.991423	Upland forest*	H1, H2, L	6.1
P10	-3.35664	-52.043752	Tributary, reservoir	H2, L	5.1
P11	-3.38557	-51.978184	River channel	H1, H2, L	19.3
P12	-3.41172	-51.968102	Pasture*	H1, H2, L	6.0
P13	-3.38170	-51.984364	Seasonally flooded* forest	H2, L	7.4
P14	-3.38557	-51.978184	River channel	H1, H2, L	2.5
P15	-3.42413	-51.937447	Seasonally flooded forested island	H1, H2, L	11.0
P16	-3.29069	-51.815787	Upland forest	H2, L	20.4
P17	-3.44253	-51.954685	Upland forest	H2, L	6.2
P18	-3.15452	-51.785845	Upland forest	H2, L	58.3
P19	-3.11501	-51.779624	River channel	H1, H2, L	6.2
P20	-3.10197	-51.748847	River channel	H2, L	2.6
P21	-2.91097	-51.913989	River channel	H1, H2, L	9.0

ND - No data collected.
*vegetation not removed prior to reservoirs filling.

725

730

735

Table 2

Env	Res	Camp	Season	FCO$_2$ (µmol CO$_2$ m^2 s^{-1})	n	pCO$_2$ (µatm)			n	k_{600} (cm h^{-1})	n
						Surface	60%	bottom			
Upstream	UR	2016 - 2017	High water	4.10 ± 2.16	1	ND	ND	ND	ND	ND	ND
		2017	Low water	1.06	1	501 ± 71.32	ND	766 ± 138	3	47.94	1
River channel	XR	2016 - 2017	High water	1.27 ± 0.31	6	771 ± 56.20	ND	808 ± 205	8	26.58 ± 2.10	3
		2017	Low water	0.89 ± 0.33	4	612 ± 161	281 ± 143	871 ± 783	7	30.70 ± 24.64	3
Flooded areas	XR	2016 - 2017	High water	0.78 ± 0.38	12	1,674 ± 17.80	1,647 ± 333	2,838 ± 83.19	6	8.91 ± 3.22	1
		2017	Low water	0.47 ± 0.12	6	1,330 ± 1,210	807 ± 103	1,498 ± 203	7	15.07 ± 20.49	3
Flooded areas	IR	2016 - 2017	High water	1.08 ± 0.62	3	1,556 ± 375	1,876 ± 37.48	1,696 ± 455	5	7.13 ± 1.59	2
		2017	Low water	7.32 ± 4.07	3	1,526 ± 263	ND	2,069 ± 152	6	60.80 ± 18.02	3
Downstream the dams	UR	2016 - 2017	High water	2.89 ± 1.74	4	2,122 ± 106	1,729 ± 689	2,257 ± 42.23	4	21.86 ± 11.01	1
		2017	Low water	0.75 ± 0.01	2	663 ± 372	ND	861 ± 257	4	26.90 ± 24.69	2
Further downstream	UR	2016 - 2017	High water	1.55 ± 1.08	4	969 ± 341	ND	998 ± 316	4	13.61 ± 16.33	1
		2017	Low water	-0.07 ± 0.62	2	409 ± 137	ND	650 ± 239	4	34.86 ± 18.49	2
Overall average			High water	1.30 ± 1.01	30	1,193 ± 520	1,618 ± 525	1,372 ± 755	27	15.61 ± 8.36	9
			Low water	1.74 ± 2.94	18	877 ± 651	676 ± 276	1,191 ± 654	31	34.39 ± 17.74	13

IR – Intermediate reservoir.

ND - No data available.

UR - unaffected river channel.

XR - Xingu reservoir.

Table 3

Variables	Analysis	p-values	Effect
pCO_2 by season	$F_{1:56}$= 9.77, R^2= 0.09	0.0045	Difference among high and low water pCO_2
pCO_2 by area	$F_{3:56}$= 13.36, R^2= 0.37	0.0002	Spatial heterogeneity of pCO_2
pCO_2 by reservoir	$F_{3:56}$= 0.34, R^2= 0.009	0.817	No difference between reservoirs pCO_2
pCO_2 by depth	$F_{2:56}$= 4.06, R^2= 0.07	0.0261	pCO_2 difference according depth
FCO_2 by sampling campaign	$F_{1:28}$= 0.09, R^2= 0.01	0.779	No difference in among 2016 and 2017 high water FCO_2
FCO_2 by area on High water	$F_{3:28}$= 7.94, R^2= 0.43	0.0089	Spatial heterogeneity on FCO_2 during high water
FCO_2 by area on low water	$F_{3:17}$= 2.67, R^2= 0.14	0.08	No spatial heterogeneity on FCO_2 during the low water
FCO_2 by reservoir on high water	$F_{1:28}$= 0.32, R^2= 0.01	0.5811	No difference between reservoirs FCO_2 during high water
FCO_2 by reservoir on low water	$F_{1:17}$= 34.07, R^2= 0.61	0.0003	Difference between reservoirs FCO_2 during low water
k_{600} by area on high water	$F_{3:9}$= 2.42, R^2= 0.70	0.2043	No spatial heterogeneity on k_{600} during the high water
k_{600} by area on low water	$F_{3:12}$= 0.12, R^2= 0.03	0.9441	No spatial heterogeneity on k_{600} during the low water
k_{600} by reservoir on high water	$F_{1:9}$= 0.02, R^2= 0.01	0.918	No difference between reservoirs k_{600} during high water
k_{600} by reservoir on low water	$F_{1:12}$= 5.46, R^2= 0.45	0.09	No difference between reservoirs k_{600} during low water
Wind velocity by area	$F_{3:37}$= 6.13, R^2= 0.23	0.0034	Spatial heterogeneity on wind velocity
Wind velocity by reservoir	$F_{2:37}$= 8.40, R^2= 0.21	0.0016	Difference between reservoirs wind velocity
Sur pCO_2 x FCO_2	R: 0.80	0.009	Correlation among surface pCO_2 and FCO_2 during high water
Bot pCO_2 x FCO_2	R: 0.68	0.042	Correlation among near bottom pCO_2 and FCO_2 during high water
Sur pCO_2 x FCO_2	R: 0.71	0.012	Correlation among surface pCO_2 and FCO_2 during low water
Bot pCO_2 x FCO_2	R: 0.45	0.16	No correlation among near bottom pCO_2 and FCO_2 during low water
FCO_2 x Wind velocity on high water	R: 0.37	0.124	No correlation among FCO_2 and wind velocity during high water
FCO_2 x Wind velocity on low water	R: 0.72	0.0006	Correlation among FCO_2 and wind velocity during low water
k_{600} x Wind velocity on high water	R: 0.73	0.016	Correlation among k_{600} and wind velocity during high water
k_{600} x Wind velocity on low water	R: 0.52	0.067	No correlation among k_{600} and wind velocity during low water
Sur pCO_2 x Sur pH	R: -0.76	0.009	Negative correlation among pCO_2 and pH in the surface
Sur pCO_2 x Bot pH	R: -0.46	0.173	No correlation among surface pCO_2 and near bottom pH
Sur pCO_2 x Sur DO	R: -0.93	0.00005	Strong negative correlation among surface pCO_2 and DO
Sur pCO_2 x Bot DO	R: -0.86	0.001	Strong negative correlation among surface pCO_2 and near bottom DO
Sur pCO_2 x Sur Temp	R: 0.00	1	No correlation among surface pCO_2 and water temperature
Sur pCO_2 x Bot Temp	R: -0.27	0.44	No correlation among surface pCO_2 and near bottom water temperature
Bot pCO_2 x Sur pH	R: -0.78	0.007	Negative correlation among near bottom pCO_2 and

			surface pH
Bot pCO$_2$ x Bot pH	R: -0.63	0.047	Negative correlation among near bottom pCO$_2$ and pH
Bot pCO$_2$ x Sur DO	R: -0.83	0.002	Strong negative correlation among near bottom pCO$_2$ and surface DO
Bot pCO$_2$ x Bot DO	R: -0.86	0.001	Strong negative correlation among near bottom pCO$_2$ and DO
Bot pCO$_2$ x Sur Temp	R: 0.28	0.43	No correlation among near bottom pCO$_2$ and surface water temperature
Bot pCO$_2$ x Bot Temp	R: -0.03	0.919	No correlation among near bottom pCO$_2$ and water temperature

745

Table 4

Environment	pH	DO (mg L^{-1})	Cond (µS cm^{-1})	Temp (°C)	WS (m s^{-1})
Downstream of dams	6.62 ± 0.18	5.87 ± 1.39	29.30 ± 4.85	29.52 ± 0.09	1.66 ± 0.88
Flooded areas	6.60 ± 0.26	5.44 ± 2.00	31.60 ± 8.63	29.85 ± 0.66	1.96 ± 1.13
Unaffected river channel	6.75 ± 0.24	7.28 ± 0.73	30.59 ± 6.87	29.72 ± 0.36	2.06 ± 0.84
River channel	6.81 ± 0.21	6.92 ± 0.26	29.86 ± 5.30	29.44 ± 0.62	3.21 ± 0.89

Table 5

FCO$_2$ (µmol CO$_2$ m^2 s^{-1})		pCO$_2$ (µatm)		k_{600} (cm h^{-1})		Ref
High water	Low water	High water	Low water	High water	Low water	
ND	0.75 ± 0.41	ND	643 ± 172	ND	16.87 ± 10.36	Alin et al. 2011
2.6 ± 1.12	-0.06 ± 0.15	1,646 ± 663	377 ± 154	11.70 ± 5.45	5.175 ± 3.39	
2.3 ± 0.41	0.4 ± 0.18	2,620 ± 810	724 ± 334	8.22 ± 3.80	5.05 ± 0.77	Rasera et al. 2013
1.92 ± 0.96	0.4 ± 0.15	1,799 ± 753	1,037 ± 635	12.20 ± 4.35	7.0 ± 6.64	
1.75	0.76	450	449	ND	16.03	Sawakuchi et al. 2017

750